Green Chemistry

Controlling metal oxide nanoparticle size and shape with supercritical fluid synthesis

Journal:	*Green Chemistry*
Manuscript ID	GC-CRV-05-2019-001619.R1
Article Type:	Critical Review
Date Submitted by the Author:	19-Jun-2019
Complete List of Authors:	Lane, Mary Kate; Yale University, Chemical and Environmental Engineering Zimmerman, Julie; Yale University, Department of Chemical and Environmental Engineering

CRITICAL REVIEW

Controlling metal oxide nanoparticle size and shape with supercritical fluid synthesis

Mary Kate Mitchell Lane, [a] Julie B. Zimmerman *[a,b]

Metal oxide nanoparticles are emerging as important contributors in a variety of applications including water treatment, catalytic transformations, and energy generation and storage, among others. Controlling size and shape is of significant interest in the nanotechnology community as these are critical in determining nanoparticle performance, impacting properties such as reactivity, conductivity, and magnetic behavior. In addition to employing green solvents, supercritical fluid nanoparticle synthesis is a robust and facile method to meet the need to control size and shape for a variety of metal oxide nanoparticles. Supercritical water, supercritical ethanol, and supercritical carbon dioxide solvent systems offer tunable properties that allow for control of nanoparticle size and shape. This review investigates the synthesis routes, the mechanisms for size and shape control, and unique characteristics particular to each green solvent. Finally, a decision tree is developed to facilitate synthetic route design for the intended nano metal oxide composition, size, and shape that highlights the need for consideration of energy and life cycle impacts.

Received 00th January 20xx,
Accepted 00th January 20xx

DOI: 10.1039/x0xx00000x

1. Introduction

The recent emergence of nanomaterials with desirable and distinct catalytic, optical, chemical, and electronic properties as compared to bulk material of the same composition has the potential to enhance many critical technologies. Metal oxide nanoparticles, in particular, have been pursued for a variety of technological solutions with environmentally beneficial applications. For example, zinc oxide and titania nanoparticles have been used in water and wastewater disinfection due to their efficient and effective photocatalytic properties.[1] Titania nanoparticles have also been utilized in solar cells as semiconductors and in artificial photosynthesis for atmospheric carbon dioxide reduction.[2,3] Batteries for electric vehicles rely on cathodes with lithium metal oxide nanoparticles to obtain high operating voltages and high theoretical energy density.[4] Additionally, magnetic iron oxide nanoparticles have been applied in the remediation of polluted waters, adsorbing heavy metals from aqueous systems followed by facile separation and recovery with an external magnetic field.[1]

The functional performance of these metal oxide nanoparticles in their respective applications is strongly influenced by their structure and properties,[5] as related to their size and shape. For example, with hematite (Fe_2O_3) used in electrodes, nanorods have higher photocurrent efficiency than spherical particles due to more direct electron transport and minimization of charge-carrier recombination losses.[6] For chromium doped ceria (CeO_2) nanoparticles designed as catalysts to treat waste from the petroleum and pulp and paper industries, cubic ceria with (100) exposed facet performed better than octahedral ceria with the exposed facet of (111) by having increased oxygen storage capacity.[7] Along with shape, size is particularly important for effectiveness or desirability in applications. In catalyst applications, surface area is extremely important with smaller particles often demonstrating enhanced catalytic activity,[8] although the nature of the surface is also important contributor.[9] Size can also affect magnetic behavior: magnetite (Fe_3O_4) and maghemite (γ-Fe_2O_3) are typically ferrimagnetic, but when the particles are smaller than 10 nm, they exhibit superparamagnetic behavior. This feature allows the nanoparticle movement in systems to be controlled by an external magnetic field and minimize agglomeration when the field is removed.[8] These collective examples, among many others, demonstrate the vital need for a versatile synthesis process that can customize the size and shape of metal oxide nanoparticles to maximize their functional performance in the intended application.

In order to fully reap the technological and environmental benefits of these technologies, we must also consider the environmental impact during the nanoparticle synthesis. Supercritical fluid nanoparticle synthesis (SCF nano synthesis) can robustly and readily control size and shape of metal oxide nanoparticles, while offering a potentially greener synthetic route through the employment of green solvents.[10,11] A recent Life Cycle Assessment (LCA) of titania nanoparticles synthesis showed that SFC nano synthesis had the potential to reduce environmental and human health impacts from conventional precipitation synthesis based on preliminary lab scale comparison.[12]

SCF nano synthesis controls nanoparticle features by utilizing the unique properties associated with solvents in their

[a] Chemical and Environmental Engineering, Yale University, 17 Hillhouse Ave, New Haven, CT 06511
[b] School of Forestry and Environmental Studies, Yale University, 195 Prospect Street, New Haven, CT, 06511
*Corresponding author

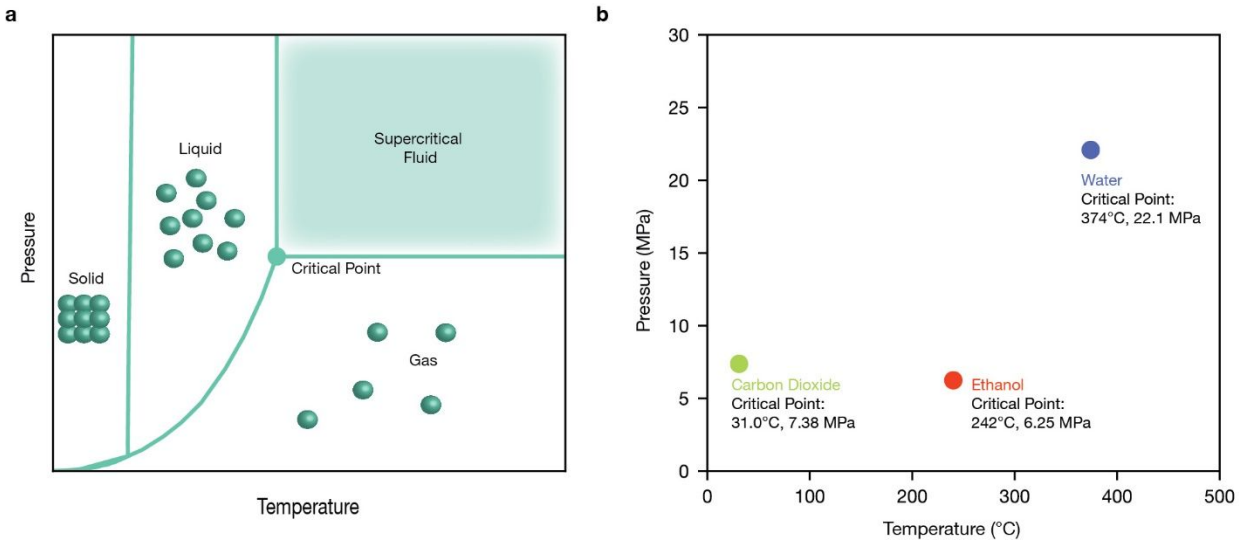

Fig. 1 (a) Generic phase diagram highlighting the supercritical fluid region. (b) Critical temperatures and pressures for water,[13] ethanol,[14] and carbon dioxide.[15,16]

supercritical state. The supercritical state is achieved when a substance is at a temperature and pressure above its critical point (Figure 1a). In this state versus the subcritical state, the supercritical fluid has drastically different properties (*e.g.*, density, dielectric constant, solubilizing capacity) that can be exploited for nanoparticle synthesis. Furthermore, since the supercritical state is achieved through changes in temperature and pressure, the system can be easily tuned to the optimal set point(s) that will yield the desired nanoparticle features. This review focuses on three main solvents used in SCF nano synthesis: water, ethanol, and carbon dioxide because control of nanoparticle size and/or shape in each of these systems has been successfully demonstrated.

While controlling nanoparticle size and shape, SCF nano synthesis enables a greener synthetic route. Currently, many conventional metal oxide nanoparticle synthetic methods rely on extremely high temperatures or toxic reagents followed by separation, purification, and/or crystallization processes. For example, sol-gel methods of titania (TiO_2) nanopowders use organic solvents such as toluene,[8] surfactants and ionic liquids,[17] and/or chemical additives that require additional steps to remove, increasing the energy consumption of the process and time required, typically through annealing/calcination processes at or above 250°C for two hours or more.[3,18] Some colloidal synthesis methods of lanthanide-doped vanadates (YVO_4:Eu) require heat treatments of two hours at 500°C for complete removal of organic polymers and ten minutes at 1000°C for proper crystallization.[19] In contrast, SCF nano synthesis employs green solvents: water, ethanol, and carbon dioxide ("green" due to minimal to no environmental, health, and safety concerns, minimal to no emissions, and abundant in the environment or renewably sourced).[20] Water, ethanol, and carbon dioxide all have accessible critical points (Figure 1b) and oftentimes can generate crystalized complexes in-situ which make them less energy intensive than methods with additional calcination post-treatment.

SCF nano synthesis can be used to produce a variety of metal oxide nanoparticles with controlled size and shape offering a valuable method to yield specific materials as dictated by the intended functional use. This review investigates the synthetic routes, the mechanisms for size and shape control, and unique characteristics particular to each solvent. Finally, a decision tree is developed to facilitate synthetic route design for the intended nano metal oxide composition, size, and shape while examining the environmental impact of the process.

2. Supercritical Water

Through supercritical hydrothermal synthesis, supercritical water (scH_2O) has been successfully demonstrated in the production of a variety of metal oxide nanoparticles (*e.g.*, AlOOH,[21] Al_2O_3,[21] CeO_2,[22-24] Co_3O_4,[25] CuO,[21] Fe_2O_3,[26-29] Fe_3O_4,[27-29] $Gd(OH)_3$,[30] MnO_2,[31] Mn_2O_3,[31] NiO,[21] SnO_2,[32] TiO_2,[2] ZnO,[33,34] ZrO_2[21]). In addition to single metal oxides, scH_2O can produce mixed metal oxides with controlled composition in a single step through introducing mixed metal precursor streams directly into supercritical hydrothermal synthesis process (e.g., $BaTiO_2$,[35] $Ba_{0.6}Sr_{0.4}TiO_3$,[36] $CoFe_2O_4$,[37] $Ce_{1-x}Zr_xO_2$,[38,39] La_2CuO_4,[40] $LiCoO_2$,[41] $LiMn_2O_4$,[42] $NiFe_2O_4$,[37] $Ni_xCo_{1-x}Fe_2O_4$,[37] where x varies from 0-1. Note: For mixed metal oxides, the addition of a base is sometimes needed to alleviate inconsistent reactivities of the differing metals.[43])

Supercritical hydrothermal synthesis of metal oxides occurs in two steps: first hydrolysis of the hydrated metal ion into a metal hydroxide (Equation 1) then condensation or precipitation of the metal oxide from the metal hydroxide (Equation 2).[7,22,24,44]

$$MA_x + xH_2O \rightleftharpoons M(OH)_x + xHA \quad [1]$$

$$M(OH)_x \rightleftharpoons MO_{\frac{x}{2}} + \frac{x}{2}H_2O \quad [2]$$

where M is the metal cation, A is the anion or ligand, and x denotes stoichiometry.

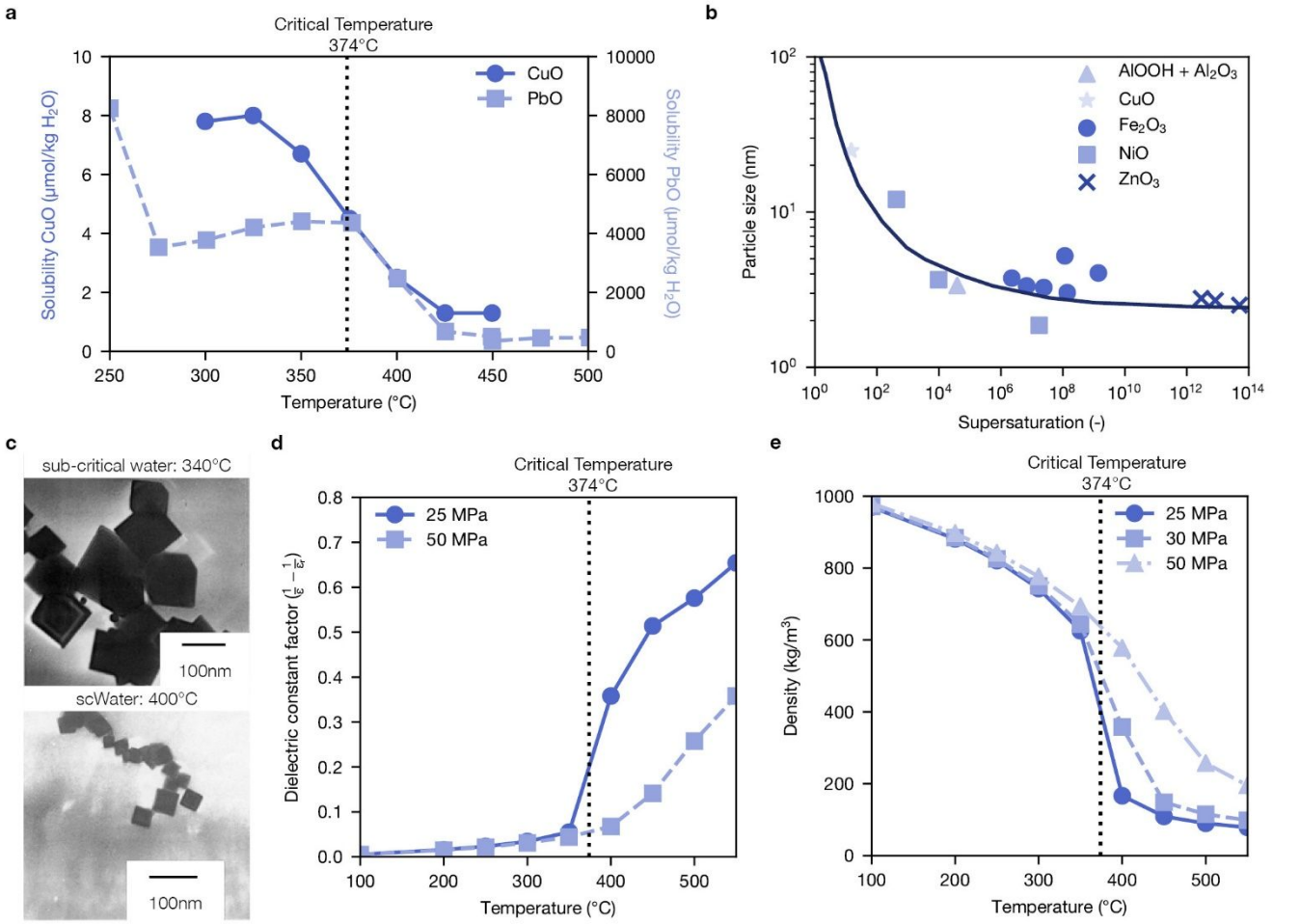

Fig. 2 (a) Solubility of metal oxides as a function of temperature (CuO at 28 MPa, PbO at 30 MPa).[45] (b) Particle size as a function of supersaturation (solubility), for synthesis at 400°C for 1 second.[21] (c) SEM pictures of ceria nanoparticles, larger particles produced in sub-critical water at 340°C and smaller particles in scH_2O at 400°C.[46] (d) Dielectric constant factor of water as a function of temperature and pressure.[47] (e) Density of water as a function of temperature and pressure.[48]

2.1. Controlling Size in Supercritical Water

For size control in scH_2O, the reaction rate and the solubility of the metal oxide are the most important factors contributing to the final size of the nanoparticles; with the faster the reaction rate and the lower the solubility of the metal oxide, the smaller the nanoparticles, based on nucleation theory.[22,49] Only once the concentration of the metal oxide monomer is above the saturation point does nucleation of nanoparticles occur. Interestingly, in subcritical water this occurs gradually allowing dissolution and Ostwald ripening, where smaller particles deposit onto larger particles. As the solubility of the metal oxide is higher in subcritical water, this further enables this process of dissolution, re-crystallization, and Ostwald ripening. In contrast, the nucleation rate in scH_2O is extremely fast, sometimes over 1000 times faster than subcritical conditions, and solubility drops considerably (Figure 2a) resulting in a high degree of supersaturation and smaller nanoparticles sizes (Figure 2b).[21,44,46] Adschiri *et al.* synthesized a range of sizes of cubic ceria nanoparticles in water at temperatures ranging from 250°C to 400°C, achieving average particle sizes greater than 200 nm at the lower temperature range and less than 20 nm at the higher temperatures (Figure 2c).[46] Tunability for size can also be within a narrow range depending on the system, with spherical titania nanoparticles 3 nm in diameter produced at 225°C and 7 nm produced at 475°C.[50]

The significant decrease in dielectric constant of scH_2O from subcritical to supercritical conditions contributes to the increased reaction rate and decreased metal oxide solubility at supercritical conditions as described by the Born equation (Equation 3). This equation, which is often used to model the overall rate of reaction during supercritical hydrothermal synthesis, describes reaction rate as a function of temperature and the dielectric constant of water.[44,46]

$$lnk = lnk_0 - \frac{E}{RT} + \frac{\varphi}{RT}\left(\frac{1}{\varepsilon} - \frac{1}{\varepsilon_r}\right) \qquad [3]$$

where Ψ is a constant determined by a reaction system, ε is the dielectric constant, k_0 is the reaction rate at dielectric constant ε_r, R is the gas constant, T is in Kelvin, and $\left(\frac{1}{\varepsilon} - \frac{1}{\varepsilon_r}\right)$ is referred to as the dielectric constant factor. Low dielectric constant (or high dielectric constant factor) is known to increase the chemical potential of ions and suppress the dissolution of metal oxide, decreasing the solubility.[46] Noticeably, the dielectric constant factor rapidly increases once water enters the supercritical

state thereby increasing the hydrolysis rate, directly affecting particle size (Figure 2d).[22]

In continuous hydrothermal synthesis versus batch, another key factor that affects size is mixing. While the chemistry of the reaction dictating size still holds true, mixing a metal oxide precursor stream with a preheated scH_2O stream is not always ideal in practice. Darr *et al.* notes that although the supercritical water stream may initially be above the critical point, mixing with an ambient temperature precursor stream can cause instances of lower temperature as nanoparticles are forming, affecting the actual size and widening the particle size distribution (PSD).[51] Kawasakie *et al.* observed these phenomena when synthesizing NiO nanoparticles in a T-shaped mixer. By increase flowrate from 30 to 60 g/min, which increased mixing, particle size decreased from 54.3 nm to 20.1 nm.[52] Due to the differences in mixing, the actual conditions experience in each synthesis were different resulting in differing average particle sizes. In a ceria nanoparticle synthesis, differing arrangements of the inlet streams and outlet stream of a T-shaped reactor affected average particle size as well as PSD.[53] Because of this, efforts to design continuous reactors with improved mixing from the standard T-shaped mixer have produced Y-shaped mixers,[54] nozzle mixers,[55] confined jet mixers,[56] counter-current mixers,[57] and a swirl mixer,[51] among others. These different configurations impact mixing efficiency and effectiveness, and subsequently, overall nanoparticle quality. In a nozzle type mixed reactor, ceria BET surface areas that are reflective of particle size were in the range of 90 ± 5 m^2/g. While in a T-shaped mixed reactor, surface area fluctuated unpredictably between 52 and 104 m^2/g, indicating a larger PSD.[55] The ability to understand and improve mixing has been essential in the scale up and commercialization of scH_2O synthesis.[43]

2.2. Controlling Shape in Supercritical Water

Supercritical water can also be used to control for shape and crystallite phase of nano metal oxides through changes in density, which decreases sharply from subcritical to supercritical conditions (Figure 2e).[22] For example, zinc oxide synthesized under subcritical water conditions (335°C, 13.7 MPa) at a density of 84.3 kg/m^3 showed crystal growth in the [001] direction forming nanorods and nanowhiskers 10-100 nm in diameter and up to 50 µm in length.[58] Alternatively, under supercritical water conditions (468°C, 25.8 MPa) with a density of 7.72 kg/m^3, ZnO displayed equiaxial and dendrite growth forming spherical-like particles 20-100 nm in diameter and branched structures with an average cross-section of 100 nm and lengths up to 2 µm.[58] Chromium-doped ceria nanoparticles were octahedral with exposed (111) facets when synthesized at 750 kg/m^3 (300°C, 28 MPa) and were cubic with exposed (100) facets when synthesized at 260 kg/m^3 (400°C, 28 MPa).[7] Control of shape and exposed facet is particularly important in the performance of ceria nanoparticle catalysts with (100) surface being the most active site suggesting that the cubic shape is the more desirable for that particular function. Barium titanate nanoparticles formed under water densities greater than 520 kg/m^3 resulted in cubic $BaTiO_3$, while supercritical conditions with water densities less than 470 kg/m^3 yielded tetragonal $BaTiO_3$.[59] Noguchi *et al.* reported that aluminum metal oxide synthesis from aluminum nitrate favors formation of spinel γ-Al_2O_3 at lower water densities, such as 250 kg/m^3, while at higher densities, such as 360 kg/m^3, formation γ-AlOOH with more tetrahedral cation sites is favored.[60] These densities correspond with only 10°C difference in temperature, from 410°C to 400°C, but greatly alter the nanoparticle product.[61] These differing morphologies are attainable due to the precipitous decrease of water density at supercritical conditions (Figure 2e), thereby increasing the rate at which dehydration or dehydroxylation occurs (Equation 2). Increasing the dehydration rate reduces residual OH ions in the crystal lattice allowing γ-AlOOH to convert to spinel γ-Al_2O_3 or cubic $BaTiO_3$ to convert to tetragonal $BaTiO_3$.

2.3. Supercritical Water Modeling

In addition to experimental work, several groups have modeled scH_2O synthesis of metal oxide nanoparticles such as CeO_2, AlOOH, TiO_2, Bi_2O_3, ZrO_2, among others.[24,35,44,62-64] Incorporating system conditions such as pressure, temperature, pH, and precursor concentration with thermodynamic and/or chemical models can pinpoint optimal operating conditions and predict particle size distributions based on the speciation of precursors and solubility of metal oxides in sub- and supercritical water. These studies indicate that pH is a tunable parameter in addition to temperature and pressure that can affect the final metal oxide nanoparticle. Significant work has been completed on modeling continuous flow reactors and investigating mixing parameters and configurations to achieve the most optimal mixing.[52,65-69] These have typically been CFD modeling, but also Blood *et al.*'s work that used light adsorption imaging and model fluids to visually analyze mixing points.[69] As scH_2O synthetic processes are designed, understanding the supercritical hydrothermal system via modeling becomes increasingly important to realize the desired size and shape characteristics of metal oxide nanoparticle products without numerous empirical trials.

2.4. Applications of Supercritical Water Synthesis

scH_2O synthesis has been successfully applied at many scales, from batch, to continuous, pilot scale,[70-72] and most recently full commercial scale.[73] Over the last decade, Hanwha Chemical developed a commercial plant producing 600 tons per year of $LiFePO_4$ in the form of platelets with an average particle size of 350nm.[54,70,74] Hanwha Chemical's scH_2O synthesis is reported to have a narrower particle size distribution compared to other commercial companies employing subcritical hydrothermal synthesis.[74] Additionally, Promethean Particles scaled their pilot process to a continuous multi-material nanoparticle manufacturing plant, producing more than 1000 tons of designed inorganic nanoparticles per year with the flexibility to switch between types of metal oxides produced.[54,73]

Whether in batch or commercial scale, scH_2O regulates the size of metal oxide nanoparticles through increased reaction rate and decreased solubility of the metal oxide dictated by tunable process set points of temperature, pressure, pH, and

mixing. scH_2O can control shape through its extreme changes in density. Furthermore, experimental scH_2O synthesis conditions as well as modeling tools exist in literature for many metal oxides, many sizes, and many shapes, making it a robust and adaptable method for metal oxide nanoparticle synthesis.

3. Supercritical Ethanol

Solvothermal synthesis in supercritical ethanol (scEtOH) is similar to hydrothermal synthesis in supercritical water but involves an additional pre-step, where the ethanol condenses under supercritical conditions to produce water which subsequently reacts (Equations 4-6) to form metal oxide nanoparticles.[75]

$$2x\ C_2H_5OH \rightleftharpoons x\ C_2H_5OC_2H_5 + x\ H_2O \quad [4]$$

$$MA_x + x\ H_2O \rightleftharpoons M(OH)_x + x\ HA \quad [5]$$

$$M(OH)_x \rightleftharpoons MO_{\frac{x}{2}} + \frac{x}{2} H_2O \quad [6]$$

scEtOH is advantageous in some cases over scH_2O because it does not immediately react with precursors making it a milder reagent and allowing for greater tunability in process design while requiring less energy inputs from a lower critical point.[76] Polar solutes, like metal chlorides which are common precursors for metal oxides, exhibit high solubility in scEtOH, unlike scH_2O and $scCO_2$.[77] Further, through in-situ crystallization of high purity nanoparticles, scEtOH can obviate additional synthesis and processing steps necessary in other synthesis routes. For example, Reverón *et al.* directly produced high purity $BaTiO_3$ and barium strontium titanate nanoparticles in a single-step through the scEtOH solvothermal process. To achieve high purity $BaTiO_3$ through other methods like the Pechini type reaction or high gravity reactive precipitation requires extensive post-processing to remove solvents, by-products, and impurities like $BaCO_3$, while low temperature solvothermal methods require additional calcination to realize the desired crystallinity.[36,78]

scEtOH can act as both a solvent and a reducing agent at supercritical conditions. This has been exploited in the synthesis of metal nanoparticles, such as Cu, Ni, and Ag, since they could not be produced in scH_2O unless substantial amounts of reducing agents were added.[79] In metal oxide formation, scEtOH is a preferred solvent when a reduction of the precursor is needed. For example, Abdeen *et al.* used scEtOH to reduce FeS and Fe_2O_3 particles into stable phase magnetic nanoparticles, Fe and Fe_3O_4, that were spherical in shape and had narrow size distributions, 18±2 nm and 50±1 nm, respectively.[80] Lui *et al.* reduced VOC_2O_4 to yield V_2O_3 nanoparticles that were spherical in morphology, with a narrow size distribution, and high purity.[81] This study illustrated the importance of operating at supercritical condition; at subcritical ethanol conditions, V_2O_3 nanoparticles did not have a uniform size distribution and were of irregular shape (Figure 3a-b). The yield of more controlled and higher quality nanoparticles at supercritical conditions may be due to a faster nucleation rate that reduces the potential for Ostwald ripening which can cause inconsistent growth. Instead, particles nucleate rapidly and concurrently allowing growth to occur more consistently.

In addition to crystallinity and purity, synthesis in scEtOH can enhance the performance of nanoparticles through precise size control. When synthesizing $NiFe_2O_4$ nanopowders, magnetic performance is strongly dependent on particle size, with a critical crystallite size around 100 nm.[82] Ćosović *et al.* synthesized particles with crystallize sizes of 81 nm in subcritical ethanol (*e.g.*, 200°C and 3.37 MPa) and 108 nm in scEtOH (*e.g.*, 260°C and 7.27 MPa); both syntheses included a post-treatment, annealing at 900°C for 4 hours.[82] scEtOH also yielded nanoparticles with higher $NiFe_2O_4$ purity and lower α-Fe_2O_3 contamination; this, along with close to ideal crystallite size, lead to improved hysteresis loops and magnetic properties.[82] It is also worth noting that when compared to other synthesis methods (*e.g.*, co-precipitation from chlorides at 145°C in N_2 atmosphere, using ethylene glycol as solvent and capping agent; hydrothermal method at 120°C with nickel dodecyl sulfate, $FeCl_3$, and NaOH; chemical combustion with ethylene glycol; combustion method with microwave heating) the magnetic properties, coercivity and remanence, were greatly improved in both the sub- and scEtOH synthesis. This is most likely due particle formation close to the critical size of 100 nm without sacrificing purity. Similar to scH_2O, the density of scEtOH, which varies greatly from the subcritical to the supercritical range, can be tuned by temperature and pressure (Figure 3c).[83] Because of this tunability, it would follow that size could be controlled in a similar fashion in scEtOH as in scH_2O, although additional experiments are required to confirm this.

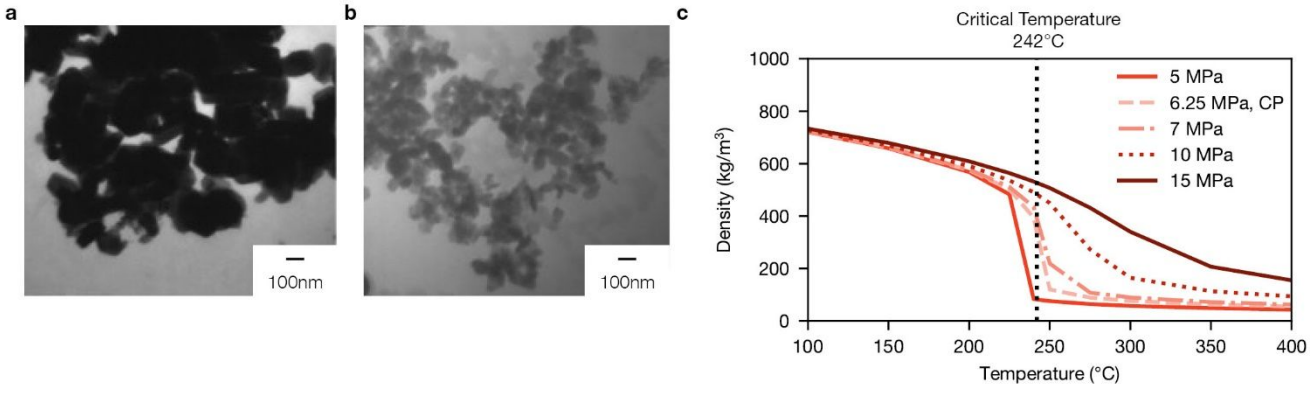

Fig. 3 TEM images of V2O3 nanoparticles at subcritical and supercritical conditions: (a) 220 °C, 5.4 MPa; (b) 242 °C, 6.5 MPa.[81] (c) Density of ethanol as a function of temperature and pressure.[83]

4. Supercritical Carbon Dioxide

As discussed, supercritical nanoparticle synthesis requires a high precursor solubility to enable high yields and a low metal oxide solubility to enable small particles. Metal salt and metal nitrate precursors that are popular in scH_2O and scEtOH are generally not soluble in pure carbon dioxide.[84] Instead, supercritical carbon dioxide ($scCO_2$) can solubilize many types of organometallic precursors that cannot typically be utilized in scH_2O or scEtOH.[84,85] With densities similar to liquid carbon dioxide (Figure 4a), $scCO_2$ retains similar solvation power. Solubility of organometallic precursors increases as carbon dioxide densities increases, with high solubility only attainable at liquid or $scCO_2$ densities (Figure 4b). Peng et al. and Gougousi et al. reported exploiting the solvent properties of $scCO_2$ to deposit thin film metal oxide coatings from organometallic precursors onto carbon nanotubes and silica substrates respectively.[86,87] $scCO_2$ can also facilitate deposition of nanoparticles onto polymer matrices, like in the case of palladium impregnated Nafion membranes.[88] Most recently, Zefirov *et al.* reported synthesis of manganese oxide nanoparticles in $scCO_2$ from an organometallic precursor, which when compared to particles synthesized under similar pyrolysis conditions, were smaller by an order of magnitude (42 nm vs 460 nm), had much higher uniformity and specific surface area, and were of a rod-like shape instead of spherical.[89] Zefirov *et al.* attributed these results to a "delayed precipitation" effect occurring in the $scCO_2$, where a $scCO_2$-enabled stabilizing organic shell around the growing inorganic nanoparticles prevents their interaction and clustering.[89] That is, the nanoparticle grows inside the organic shell and precipitates once it exceeds the size of the shell (Figure 5) where the size of

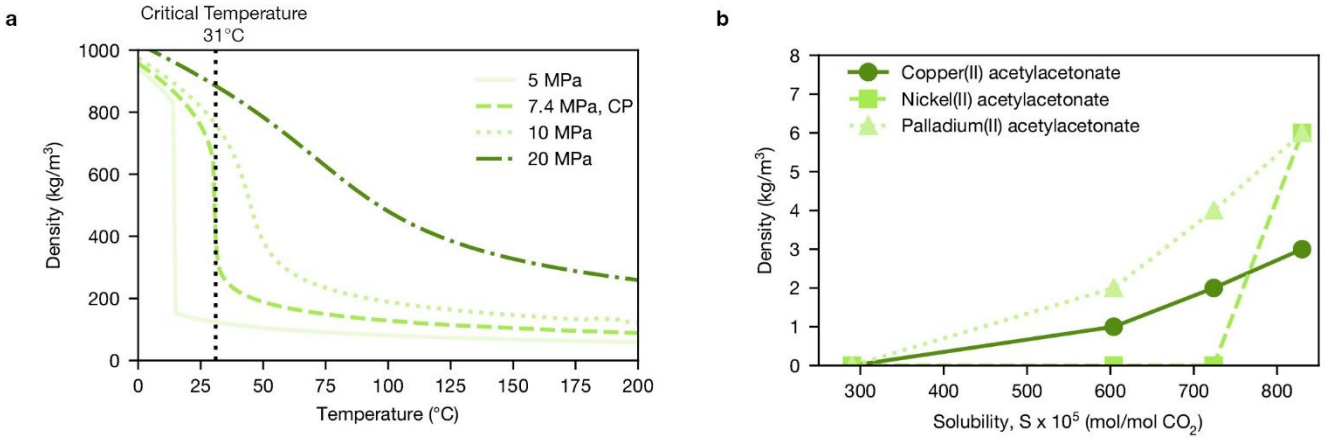

Fig. 4 (a) Density of $scCO_2$ as a function of temperature and pressure.[90] (b) Solubility of organometallic precursors as a function of $scCO_2$ density.[91]

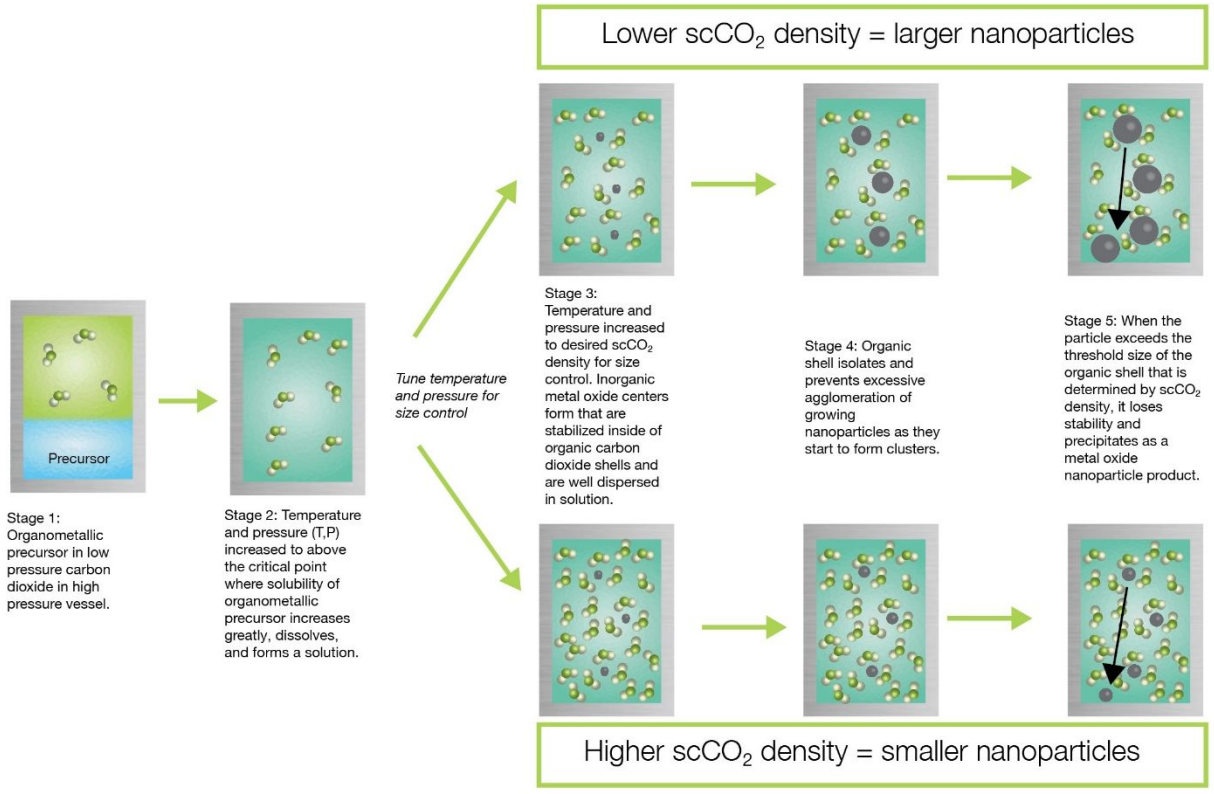

Fig. 3 Formation of size-controlled nanoparticles in $scCO_2$ through delayed precipitation.[89]

the organic shell can be tuned by changing density of $scCO_2$ through process parameters (e.g. temperature and pressure). This suggests that $scCO_2$ can be used in the controlled synthesis of metal oxide nanoparticles derived from organometallic precursors by manipulating size through changes in density. A comprehensive list of organometallic precursors, including Cu, Fe, Ni, Zn, Mn, Ti, and other metal-based compounds, and their solubility in $scCO_2$ was reviewed by Teoh *et al.*,[91] which can be useful in designing $scCO_2$ nano synthesis processes for nano metal oxides.

Additional advantages of $scCO_2$ include liquid-like diffusivity, gas-like viscosity, and near zero surface tension, which all contribute to increased reaction kinetics and allow for enhanced conditions for chemical reactions on the surface and reduced surface tension driven effects.[92,93] As a solvent, $scCO_2$ is easily separable from the nanoparticle product through just releasing the pressure with no additional separation or drying steps. Additionally, the electrochemical inertness of carbon dioxide limits undesirable reactions between solvent and the precursor(s) that can occur in purely solvothermal synthesis methods, like carbonate contamination in scEtOH systems.[89]

5. Supercritical Solvent Mixtures

Several studies have reported synergistic effects from solvent mixtures (*e.g.*, water, carbon dioxide, and ethanol), where the synthesis conditions are above at least one of the critical points. Utilizing $scCO_2$ in hydrothermal synthesis reduces the energy demand by allowing process conditions below the critical point of water, but above the critical point of carbon dioxide while still producing a crystalline product. This $scCO_2$-water combined system retains the solvent benefits of water and incorporates the tunable density of $scCO_2$. Size control in $scCO_2$-water systems is similar to the delayed precipitation process, but instead of dissolving in $scCO_2$, the precursor dissolves in the water with the density of $scCO_2$ restricting agglomeration and dictating maximum size of the nanoparticles in a $scCO_2$-water emulsion type system.[92] Hertz *et al.* exemplifies this by establishing a direct relationship between particle size and CO_2 density in the production of titania using titanium tetrabutoxide and water as reactants.[3] Mean pore diameter decreased from 120 nm to 80 nm to 55 nm as $scCO_2$ density increased from 250 kg/m^3 to 280 kg/m^3 to 330 kg/m^3 through changes in temperature at a constant pressure of 30 MPa.[3]

Different morphologies, in addition to size control, have also been attained in $scCO_2$-water systems. ZnO nanoparticles with flower-sheet morphology were formed in $scCO_2$ utilizing zinc nitrate hexahydrate and water as reactants, where crystallinity was improved through calcination post-treatments.[94] Kinoshita *et al.* reported synthesis in $scCO_2$ of titania nanoparticles with the same concentrations of titanium tetrabutoxide and acetic acid as reactants at near supercritical boundary (313 K, 20 MPa) and in the supercritical region (333 K, 20 MPa) yielding spherical and needle-like nanoparticles, respectively. While the density of $scCO_2$ changes by only 14% with these changes in temperature and pressure, very different morphologies were observed. Interestingly, with increased concentrations of starting materials at 333 K the titania had a hollow urchin-shaped morphology.[95] While the mechanism of shape control is not as well understood as size control, $scCO_2$ density and precursor/reactant concentrations in water are indicated as the main contributing factors for shape determination based on these examples.

In contrast to the immiscibility of water in $scCO_2$ just described, the miscibility of ethanol in $scCO_2$ is advantageous for metal oxide nanoparticle synthesis. For example, the solvation of $scCO_2$, which typically has limited solvent power for polar solutes, can be greatly improved with small additions of ethanol, ranging from as little as 1% to 10%.[96] At varying mole fractions of ethanol (Figure 6), carbon dioxide-ethanol systems are generated where, depending on the pressure and temperature, one-phase supercritical mixture (above mixture critical point), one phase liquid mixture or two-phase (liquid ethanol in $scCO_2$) $scCO_2$-ethanol systems form.[97] Along with the tunability of $scCO_2$ described earlier, $scCO_2$-ethanol combined systems allow for enhanced solubility tuning by varying the mole fraction of each solvent. Tenorio *et al.* studied the solubility of a nickel precursor in a $scCO_2$-ethanol system and found that $Ni(NO_3)_2{\cdot}6H_2O$ was not soluble in pure CO_2 but was soluble when ethanol was added. Tenorio *et al.* recommend a mole fraction of 0.1 ethanol for practical miscibility at moderate pressures.[98] Similar calculations and studies can be performed to optimize the amount of ethanol to solubilize other precursor/metal oxide systems for synthesis in $scCO_2$-ethanol combined systems.

Another example of the synergistic effects of a combined supercritical solvent system is scH_2O-scEtOH system in the study by Reverón *et al.* investigating the synthesis of $BaTiO_3$ from barium and titanium isopropoxides.[78] In the synthesis of $BaTiO_3$, $BaCO_3$ contamination is a common problem that adversely affects electroceramic properties and has to be removed through a time-consuming and environmentally-costly washing process using formic acid. To reduce contamination, Reverón *et al.* mixed the precursor stream of isopropoxides in ethanol before introducing water at temperature and pressure as the primary solvent. Without ethanol, introducing the

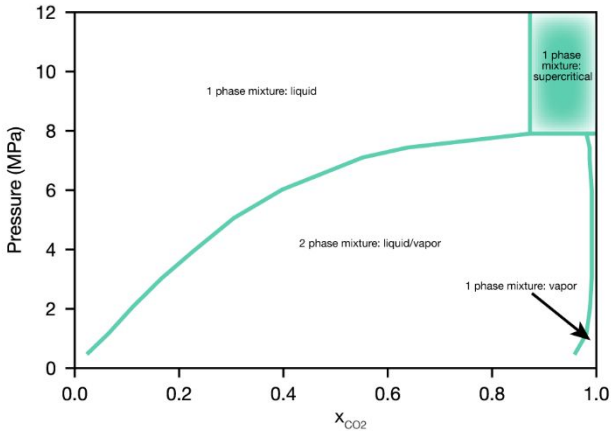

Fig. 4 Pressure-mole fraction phase diagram for an ethanol and carbon dioxide binary system at 313 K, illustrating a mixture critical point and supercritical zone.[16, 99]

isopropoxides separately favored $BaCO_3$ formation; however, using ethanol as the primary solvent still resulted in relatively high $BaCO_3$ contamination. It was through the addition of small amounts of ethanol (0.02-0.14 wt% H_2O/EtOH) to a pure water solvent stream, $BaCO_3$ contamination was greatly minimized or eliminated. Further synergies arise with the presence of water as the hydrolysis and condensation of the metal oxide occurs more rapidly than in pure ethanol and reduces the amount of time for side reactions and contaminants to form resulting in higher purity products.

6. Design of Supercritical Fluid Nanoparticle

Table 1. Comparison of the SCF nano synthesis methods investigated: supercritical water, supercritical mixtures.

production of high quality nanoparticles with tunable size and morphologies, with scH_2O, scEtOH, and $scCO_2$ having unique features in terms of energy requirements, precursor candidates, and developed computational models contributing to a variety of advantages and drawbacks for each solvent system (Table 1). It is important to note that many metal oxide nanoparticles can be formed in any of the supercritical fluid systems while controlling for size and shape characteristics compelling the question of when to use one solvent system over the other. Accordingly, a Decision Tree was developed to facilitate SCF nano synthesis design from solvent selection to system conditions depending on the desired final nano metal oxide size and shape for the intended function (Figure 7)

	scH_2O	*scEtOH*	*$scCO_2$*	*Supercritical solvent mixtures*
Energy Requirement	High Energy Requirement based on Critical Point: 374°C, 22.1 MPa	Moderate Energy Requirement based on Critical Point: 242°C, 6.25 MPa	Low energy requirement based on Critical Point: 31.0°C, 7.38 MPa (operation temperatures usually higher than critical point to achieve adequate crystallization, typically >150°C)	Typically, lower energy requirement with $scCO_2$ mixtures
Synthesis route	Hydrothermal (Equations 1-2)	Solvothermal (Equations 4-6)	Delayed precipitation (Figure 5)	Combination of synthesis routes
Types of precursor	Many types of precursors: metal nitrates, chlorides, among others; precursors that need to be oxidized	Polar solutes like metal chlorides; precursors that need to be reduced	Organometallic precursors	Flexibility in precursor choice based on combination
Size and shape control	Yes	Yes	Yes	Yes
Modeling available?	Yes, several studies[22,35,44,52, 62-64, 65-69]	None for SCF nano synthesis	Limited studies for SCF nano synthesis[100,101]	None for SCF nano synthesis
Advantages	Fast reaction time; Oxidizer; Conditions for sizes and shapes of many types of metal oxides available in literature	Can act as reductant; single-step crystallization	Can be used in combination with ethanol or water to lower energy requirements; chemical inertness reduces byproduct contamination	Synergistic effects from combinations; can use benefits of both solvents
Shortcomings	High energy requirement; reactors cannot be made of stainless steel (need scH_2O P,T rated alloy)	Higher risk for carbonate contamination	Few studies using only $scCO_2$ and precursor	More complexity in synthesis

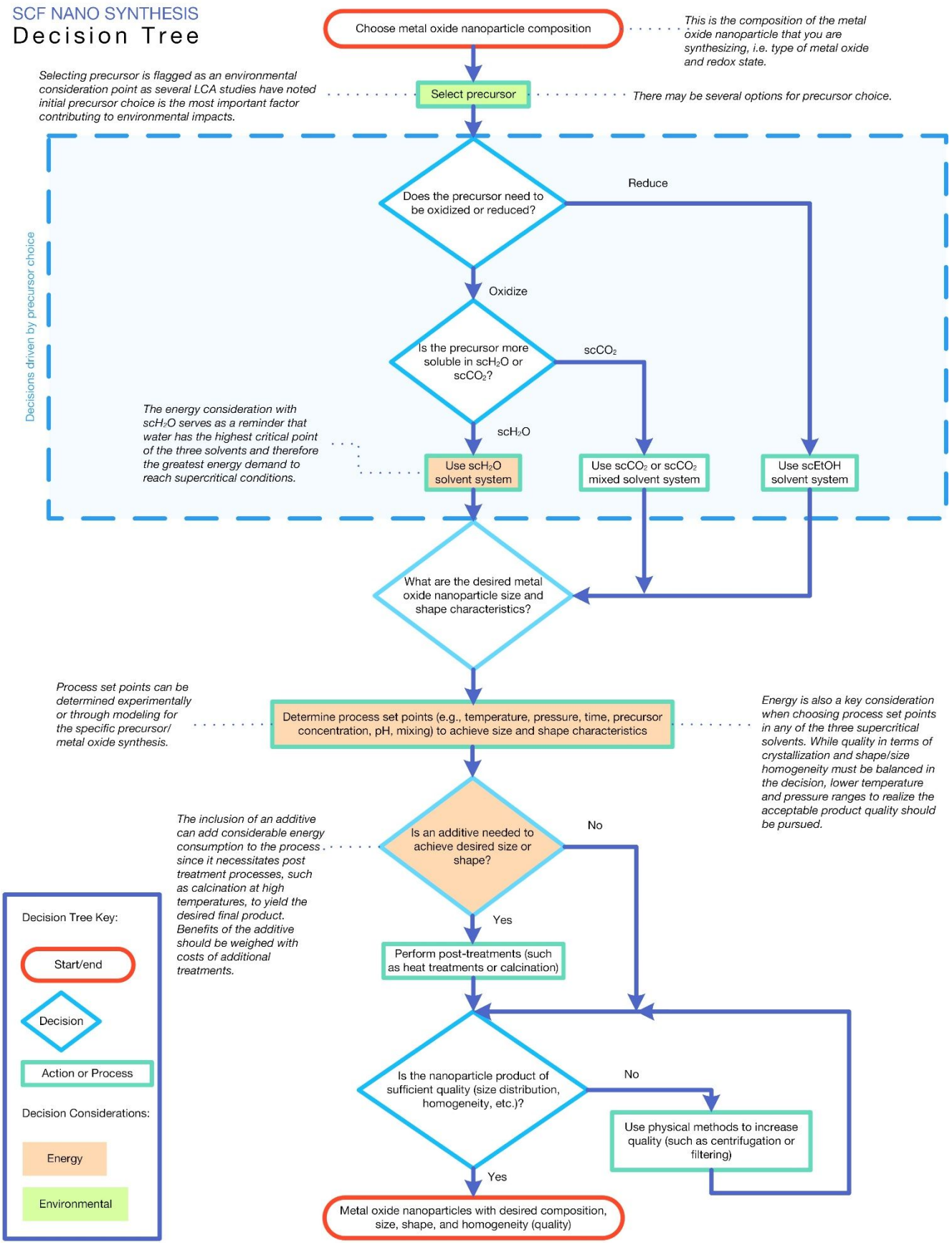

Fig. 5 Decision tree to design supercritical fluid synthesis to produce metal oxide nanoparticles, including relevant environmental and energy considerations.

6.2. SCF Nano Synthesis Decision Tree

Initially, the composition and redox state of the desired metal oxide nanoparticles (*e.g.*, FeO, Fe_2O_3, or Fe_3O_4) is determined based on the application. From this a precursor is selected. Previous studies often found that for many nano metal oxides, there are variety of viable precursors. Selection often depended on demonstrated success as a precursor for specific characteristics, fit with the chemistry of solvent or synthesis procedure, cost of precursor, and/or environmental impacts (environmental impacts explained more in depth below). Using titania as an example, precursors include titanium tetrachloride, titanium oxy-sulfate, alkoxides like titanium isopropoxide, and water soluble titanium complexes like titanium bis(ammonium lactacto) dihydroxide, among others.[102] Titanium bis(ammonium lactacto) dihydroxide would be selected for demonstrated success in producing nano titania at the pilot level in a continuous-flow hydrothermal synthesis with supercritical water. Other water-soluble titanium complexes would be selected if process was pre-determined to be a supercritical water synthesis. Titanium tetrachloride and titanium oxy-sulfate are cheaper options than organic precursors because they are easily manufactured from raw materials by mixing the source mineral with an acid solution.[102] For lowest environmental impact considering global warming potential, the choice would be titanium oxy-sulfate.[102] All of these criteria should be weighed based on the synthesis and the needs of the designer. SCF nano synthesis designers are encouraged to iterate through the decision tree with different choices of precursor to find the design that is the best fit.

After precursor selection, the chemistry of the reaction becomes important in solvent selection with the decisions driven by precursor choice. If the reaction involves a reduction of the precursor, scEtOH is a more favorable solvent over $scCO_2$ or scH_2O. If oxidation or no change in oxidation state occurs, then $scCO_2$ and scH_2O are better candidates. Deciding between $scCO_2$ and scH_2O will depend on the solubility of the precursor in each solvent system. If using an organometallic precursor, $scCO_2$ would be preferential. For a given solvent system, the size and shape of the nano metal oxide are determined by several factors including temperature, pressure, reaction time, and precursor concentration. Process set points are often determined experimentally; however, some computational modeling work has been completed for some solvent systems within certain operational parameter ranges (Table 1). An additional consideration in realizing the desired size and shape is the use of additives, which are sometimes necessary for complicated morphologies. Notably, the inclusion of an additive usually requires a post treatment step to remove the additive from the nanoparticle products. Finally, homogeneity and quality of the product metal oxide nanoparticles is considered. While “high quality” or “homogenous” are variable in definition in previous studies, here, it broadly means the nanoparticles are in the desired size range with an acceptable standard deviation as well as having an acceptable uniformity in shape. These ranges will vary between nano metal oxides and applications. If the nanoparticles are not considered homogeneous, there are additional physical methods that can be utilized, like centrifugation or filtering to remove larger particles and reduce the size distribution.

Of note, several steps along the Decision Tree (Figure 7) are flagged as being a significant contributor to the environmental or energy impacts of the SCF nano synthesis. The environmental consideration flag derives from several life cycle assessments (LCA) on metal oxide nanoparticle synthesis that indicate key decision points for reducing emissions, and subsequent negative impacts.[103] Caramanzana-González *et al.* identified precursor choice as the most important factor for both cumulative energy demand (CED) and global warming potential (GWP) in their LCA for continuous flow solvo/hydrothermal syntheses of titania nanoparticles.[102] GWP increased from 2 kg CO_2 eq per kg TiO_2 to 225 kg CO_2 eq per kg TiO_2 (a 10-fold increase) at the same synthetic conditions except for using titanium oxysulfate versus titanium bis(ammonium lactato) dihydroxide as the precursor.[102] While solvent choice, process set points, and post-treatment all contribute to CED and GWP, these were found to have much smaller overall impacts and are also related to the initial precursor choice.

Energy consumption flags are noted on three steps in the Decision Tree: scH_2O solvent choice, process set points determination, and additive inclusion. The energy consideration with scH_2O serves to remind that water has the highest critical point of the three solvents and therefore the greatest energy demand to reach supercritical conditions. Energy is also a key consideration when choosing process set points in any of the three supercritical solvents. While quality in terms of crystallization and shape/size homogeneity must be balanced in the decision, lower temperature and pressure ranges to realize the acceptable product quality should be pursued. Finally, the inclusion of an additive can add considerable energy consumption to the process since it necessitates post treatment processes, such as calcination at high temperatures, to yield the desired final product. Optimally, every consideration should be made to minimize energy demand and environmental impacts while still producing the intended nanoparticles at sufficient quality.

From this Decision Tree, SCF nano synthesis represents an attractive method for metal oxide nanoparticle production by combining versatility and control. Versatility: for an assortment of metal oxides a precursor and supercritical solvent system can be selected that is advantageous to the chemistry of the synthesis. Control: through tuning process set points nanoparticles of a particular size and shape to our standards of quality can be produced. Additionally, green solvents are utilized with additional opportunities to reduce environmental impacts and energy consumption offering supercritical fluid nanoparticle synthesis further benefits over conventional nano metal oxide synthetic routes.

Conflicts of interest

There are no conflicts to declare.

Acknowledgements

This work was supported by the National Science Foundation (NSF) Graduate Research Fellowship Program and the NSF Nanosystems Engineering Research Center for Nanotechnology - Enabled Water Treatment (ERC-1449500).

References

1 H. Lu, J. Wang, M. Stoller, T. Wang, Y. Bao and H. Hao, *Advances in Materials Science and Engineering*, 2016, **2016**, 10.
2 R. Camarillo, S. Tostón, F. Martínez, C. Jiménez, and J. Rincón, *J. Chem. Technol. Biotechnol.*, 2017, **92**, 1710-1720.
3 A. Hertz, M. Drobek, C. Ruiz, F. Charton, S. Sarrade, C. Guizard and A. Julbe, *Journal of Materials Science*, 2017, **52**, 12635 - 12652.
4 M. Tanaka, T. Kageyama, H. Sone, S. Yoshida, D. Okamoto and T. Watanabe, *Nanomaterials*, 2016, **6**, 60.
5 L. M. Gilbertson, J. B. Zimmerman, D. L. Plata, J. E. Hutchison and P. T. Anastas, *Chemical Society Reviews*, 2015, **44**, 5758-5777.
6 N. Beermann, L. Vayssieres, S. E. Lindquist and A. Hagfeldt, *Journal of The Electrochemical Society*, 2000, **147**, 2456-2461.
7 T. S. Zhu Y, Seong G, Dejhosseini M, Hossain MZ, Noguchi T, Hojo D, Aoki N, Aida T, Adschiri T., *Phil.Trans. R. Soc. A*, 2015, **373**, https://doi.org/10.1098/rsta.2015.0012.
8 U. T. Lam, R. Mammucari, K. Suzuki and N. R. Foster, *Industrial & Engineering Chemistry Research*, 2008, **47**, 599-614.
9 W. Li, K. R. Yang, X. Yao, Y. He, Q. Dong, G. W. Brudvig, V. S. Batista and D. Wang, *ACS Applied Materials & Interfaces*, 2019, **11**, 5616-5622.
10 T. Adschiri and A. Yoko, *The Journal of Supercritical Fluids*, 2018, **134**, 167-175.
11 C. Aymonier, G. Philippot, A. Erriguible and S. Marre, *The Journal of Supercritical Fluids*, 2018, **134**, 184-196.
12 M. P. Tsang, G. Philippot, C. Aymonier and G. Sonnemann, *ACS Sustainable Chemistry & Engineering*, 2018, **6**, 5142-5151.
13 Pubchem.com,https://pubchem.ncbi.nlm.nih.gov/compound/962#section=Critical-Temperature-%26-Pressure, (accessed November 2018).
14 W. M. Haynes, *CRC Handbook of Chemistry and Physics*, CRC Press Inc., Boca Raton, FL, 2015.
15 Y. N. Suehiro, M.; Yamada, K.; Uematsu, M., *J. Chem. Thermodyn.*, 1996, **28**, 1153-1164.
16 K. Suzuki, H. Sue, M. Itou, R. L. Smith, H. Inomata, K. Arai and S. Saito, *Journal of Chemical & Engineering Data*, 1990, **35**, 63-66.
17 H. Kaper, S. Sallard, I. Djerdj, M. Antonietti and B. M. Smarsly, *Chemistry of Materials*, 2010, **22**, 3502-3510.
18 M. Inoue, in *Handbook of Advanced Ceramics: Materials, Applications, Processing, and Properties*, ed. S. Somiya, Academic Press, Waltham, USA, 2, 2013, 11.1.4, 927-948.
19 G. Mialon, M. Gohin, T. Gacoin and J.-P. Boilot, *ACS Nano*, 2008, **2**, 2505-2512.
20 C. Capello, U. Fischer and K. Hungerbuhler, *Green Chemistry*, 2007, **9**, 927-934.
21 K. Sue, M. Suzuki, K. Arai, T. Ohashi, H. Ura, K. Matsui, Y. Hakuta, H. Hayashi, M. Watanabe and T. Hiaki, *Green Chemistry*, 2006, **8**, 634-638.
22 H. Hayashi and Y. Hakuta, *Materials*, 2010, **3**, 3794.
23 C. Xu and A. S. Teja, *The Journal of Supercritical Fluids*, 2006, **39**, 135-141.
24 N. K. V. Nadimpalli, R. Bandyopadhyaya and V. Runkana, *The Journal of Supercritical Fluids*, 2018, **136**, 164-179.
25 E. Lester, G. Aksomaityte, J. Li, S. Gomez, J. Gonzalez-Gonzalez and M. Poliakoff, *Progress in Crystal Growth and Characterization of Materials*, 2012, **58**, 3-13.
26 M. D. d. Tercero, M. Bruns, I. G. Martínez, M. Türk, U. Fehrenbacher, S. Jennewein and L. Barner, *Particle & Particle Systems Characterization*, 2013, **30**, 229-234.
27 M. T. Liang, S. H. Wang, Y. L. Chang, H. I. Hsiang, H. J. Huang, M. H. Tsai, W. C. Juan and S. F. Lu, *Ceramics International*, 2010, **36**, 1131-1135.
28 R. Sanchis, D. Alonso-Domínguez, A. Dejoz, M. P. Pico, I. Álvarez-Serrano, T. García, M. L. López and B. Solsona, *Materials*, 2018, **11**, 1387.
29 A. A. Vostrikov, O. N. Fedyaeva, A. V. Shishkin, M. Y. Sokol and A. V. Zaikovskii, *Technical Physics Letters*, 2012, **38**, 955-958.
30 T. Sasaki, S. Ohara, M. Umetsu, T. Naka, T. Adschiri, C. Nabeta, H. Ichikawa and Y. Fukumori, *Journal of the Society of Powder Technology*, 2006, **43**, 440-444.
31 M. Kim, S.-A. Hong, N. Shin, K. H. Chae, H.-S. Lee, S. Choi and Y. Shin, *Journal of Supercritical Fluids*, 2016, **112**, 114-118.
32 Z. Fang, H. Assaaoudi, H. Lin, X. Wang, I. S. Butler and J. A. Kozinski, *Journal of Nanoparticle Research*, 2007, **9**, 683-687.
33 S. Ohara, T. Mousavand, T. Sasaki, M. Umetsu, T. Naka and T. Adschiri, *Journal of Materials Science*, 2008, **43**, 2393-2396.
34 M. Søndergaard, E. D. Bøjesen, M. Christensen and B. B. Iversen, *Crystal Growth & Design*, 2011, **11**, 4027-4033.
35 A. Testino, V. Buscaglia, M. T. Buscaglia, M. Viviani and P. Nanni, *Chemistry of Materials*, 2005, **17**, 5346-5356.
36 H. Reverón, C. Elissalde, C. Aymonier, O. Bidault, M. Maglione, F. Cansell. *Journal of Nanoscience and Nanotechnology*, 2005, **5**, 1741-1744.
37 A. Cabañas and M. Poliakoff, *Journal of Materials Chemistry*, 2001, **11**, 1408-1416.
38 A. Cabañas, J. A. Darr, E. Lester and M. Poliakoff, *Journal of Materials Chemistry*, 2001, **11**, 561-568.
39 A. Cabanas, J. A. Darr, E. Lester and M. Poliakoff, *Chemical Communications*, 2000, **11**, 901-902.
40 A. A. Galkin, B. G. Kostyuk, V. V. Lunin and M. Poliakoff, *Angewandte Chemie International Edition*, 2000, **39**, 2738-2740.
41 Y. H. Shin, S.-M. Koo, D. S. Kim, Y.-H. Lee, B. Veriansyah, J. Kim and Y.-W. Lee, *The Journal of Supercritical Fluids*, 2009, **50**, 250-256.
42 X.-w. Liu, J. Tang, X.-s. Qin, Y.-f. Deng and G.-h. Chen, *Transactions of Nonferrous Metals Society of China*, 2014, **24**, 1414-1424.
43 P. W. Dunne, E. Lester, C. Starkey, I. Clark, Y. Chen and A. S. Munn, in *Supercritical and Other High-pressure Solvent Systems: For Extraction, Reaction and Material Processing*, ed. A. Hunt, T. Attard, The Royal Society of Chemistry, London, United Kingdom, 2018, 15, 449-475.
44 N. K. V. Nadimpalli, R. Bandyopadhyaya and V. Runkana, *Fluid Phase Equilibria*, 2018, **456**, 33-45.
45 K. Sue, Y. Hakuta, R. L. Smith, T. Adschiri and K. Arai, *Journal of Chemical & Engineering Data*, 1999, **44**, 1422-1426.
46 T. Adschiri, Y. Hakuta, K. Sue and K. Arai, *Journal of Nanoparticle Research*, 2001, **3**, 227-235.
47 E. Wasserman, B. Wood and J. Brodhol, *Geochimica et cosmochimica acta*, 1995, **59**, 1-6.
48 M. P. Verma, *Computers & Geosciences*, 2003, **29**, 1155-1163.
49 T. Adschiri, Y.-W. Lee, M. Goto and S. Takami, *Green Chemistry*, 2011, **13**, 1380-1390.
50 P. W. Dunne, A. S. Munn, C. L. Starkey, T. A. Huddle and E. H. Lester, *Philosophical Transactions of the Royal Society A: Mathematical*, Physical and Engineering Sciences, 2015, **373**, DOI: 10.1098/rsta.2015.0015.
51 J. A. Darr, J. Zhang, N. M. Makwana and X. Weng, *Chemical Reviews*, 2017, **117**, 11125-11238.

52 S.-I. Kawasaki, K. Sue, R. Ookawara, Y. Wakashima, A. Suzuki, Y. Hakuta and K. Arai, *The Journal of Supercritical Fluids*, 2010, **54**, 96-102.
53 K.-i. Sugioka, K. Ozawa, M. Kubo, T. Tsukada, S. Takami, T. Adschiri, K. Sugimoto, N. Takenaka and Y. Saito, *The Journal of Supercritical Fluids*, 2016, **109**, 43-50.
54 E. Lester, P. Dunne, Y. Chen and A. Al-Atta, in *Supercritical and Other High-pressure Solvent Systems: For Extraction, Reaction and Material Processing*, ed. A. Hunt, T. Attard, The Royal Society of Chemistry, London, United Kingdom, 2018, 14, 416-448.
55 E. Lester, P. Blood, J. Denyer, D. Giddings, B. Azzopardi and M. Poliakoff, *The Journal of Supercritical Fluids,* 2006, **37**, 209-214.
56 C. Denis, C. Tighe, R. Gruar, N. Makwana, and J. Darr, *Crystal Growth & Design*, 2015, **15**, 4256-4265.
57 C. J. Tighe, R. I. Gruar, C. Y. Ma, T. Mahmud, X. Z. Wang and J. A. Darr, *The Journal of Supercritical Fluids*, 2012, **62**, 165-172.
58 A. A. Vostrikov, O. N. Fedyaeva, A. V. Shishkin and M. Y. Sokol, *The Journal of Supercritical Fluids*, 2009, **48**, 161-166.
59 Y. Hakuta, H. Ura, H. Hayashi and K. Arai, *Materials Letters*, 2005, **59**, 1387-1390.
60 S. J. Wilson, *Journal of Solid State Chemistry*, 1979, **30**, 247-255.
61 T. Noguchi, K. Matsui, N. M. Islam, Y. Hakuta and H. Hayashi, *The Journal of Supercritical Fluids*, 2008, **46**, 129-136.
62 A. Testino, I. R. Bellobono, V. Buscaglia, C. Canevali, M. D'Arienzo, S. Polizzi, R. Scotti and F. Morazzoni, *Journal of the American Chemical Society*, 2007, **129**, 3564-3575.
63 M. R. Mozdianfard, F. Masoodiyeh and J. Karimi-Sabet, *The Journal of Supercritical Fluids*, 2018, 136, 144-156.
64 F. Masoodiyeh, M. R. Mozdianfard and J. Karimi-Sabet, *Powder Technology*, 2017, **317**, 264-274.
65 P. Zielke, Y. Xu, S. B. Simonsen, P. Norby and R. Kiebach, *The Journal of Supercritical Fluids*, 2016, **117**, 1-12.
66 J. Sierra-Pallares, T. Huddle, E. Alonso, F. A. Mato, J. García-Serna, M. J. Cocero and E. Lester, *Chemical Engineering Journal*, 2016, **299**, 373-385.
67 J. Sierra-Pallares, T. Huddle, J. García-Serna, E. Alonso, F. Mato, I. Shvets, O. Luebben, M. J. Cocero and E. Lester, *Nano Research*, 2016, **9**, 3377-3387.
68 C. Y. Ma, J. J. Liu, Y. Zhang and X. Z. Wang, *The Journal of Supercritical Fluids*, 2015, **98**, 211-221.
69 P. J. Blood, J. P. Denyer, B. J. Azzopardi, M. Poliakoff and E. Lester, *Chemical Engineering Science*, 2004, **59**, 2853-2861.
70 T. Adschiri, Y.-W. Lee, M. Goto and S. Takami, *Green Chemistry*, 2011, **13**, 1380-1390.
71 N. M. Makwana, C. J. Tighe, R. I. Gruar, P. F. McMillan and J. A. Darr, *Materials Science in Semiconductor Processing*, 2016, **42**, 131-137.
72 C. J. Tighe, R. Q. Cabrera, R. I. Gruar and J. A. Darr, *Industrial & Engineering Chemistry Research*, 2013, **52**, 5522-5528.
73 Promethean Particles, https://www.prometheanparticles.co.uk/, (accessed June 2019).
74 J. Chen, *Recent Patents on Nanotechnology*, 2013, **7**, 2-12.
75 X. M. Wang and P. Xiao, *Journal of Materials Research*, 2006, **21**, 1189-1203.
76 R. Sui and P. Charpentier, *Chemical Reviews*, 2012, **112**, 3057-3082.
77 J. B. Hannay and J. Hogarth, *Proceedings of the Royal Society of London*, 1879, **29**, 324-326.
78 H. Reverón, A. Cyril, L.-S. Anne, E. Catherine, M. Mario and C. François, *Nanotechnology*, 2005, **16**, 1137.
79 J. Kim, D. Kim, B. Veriansyah, J. W. Kang and J. D. Kim, *Materials Letters*, 2009, **63**, 1880-1882.
80 M. Abdeen, S. Sabry, H. Ghozlan, A. A. El-Gendy and E. E. Carpenter, *Journal of Nanomaterials*, 2016, **2016**, 7.
81 X. H. Liu, Y. F. Zhang, S. P. Yi, C. Huang, J. Liao, H. B. Li, D. Xiao and H. Y. Tao, *Journal of Supercritical Fluids*, 2011, **56**, 194-200.
82 A. R. Ćosović, T. Žák, S. B. Glisic, M. D. Sokić, S. S. Lazarević, V. R. Ćosović and A. M. Orlović, *The Journal of Supercritical Fluids*, 2016, **113**, 96-105.
83 H. E. Dillon and S. G. Penoncello, *International Journal of Thermophysics*, 2004, **25**, 321-335.
84 M. J. Tenorio, S. Gines, C. Pando, J. A. R. Renuncio and A. Cabanas, *Journal of Chemical and Engineering Data*, 2018, **63**, 1065-1071.
85 M. Škerget, Ž. Knez and M. Knez-Hrnčič, *Journal of Chemical & Engineering Data*, 2011, **56**, 694-719.
86 Q. Peng, J. C. Spagnola, H. Daisuke, K. J. Park and G. N. Parsons, *Journal of Vacuum Science & Technology B: Microelectronics and Nanometer Structures Processing, Measurement, and Phenomena*, 2008, **26**, 978-982.
87 T. Gougousi and Z. Chen, *Materials Research Society*, 2008, **1007**, 307-312.
88 F. Cansell and C. Aymonier, *The Journal of Supercritical Fluids*, 2009, **47**, 508-516.
89 V. V. Zefirov, I. V. Elmanovich, E. E. Levin, S. S. Abramchuk, E. P. Kharitonova, A. A. Khokhlov, M. S. Kondratenko and M. O. Gallyamov, *Journal of Materials Science*, 2018, **53**, 9449-9462.
90 S. Anwar and J. J. Carroll, *Carbon Dioxide Thermodynamic Properties Handbook : Covering Temperatures from -20° to 250°C and Pressures up to 1000 Bar*, Wiley, Hoboken, USA, 2016.
91 W. H. Teoh, R. Mammucari and N. R. Foster, *Journal of Organometallic Chemistry*, 2013, **724**, 102-116.
92 X. Zhang, S. Heinonen, E. Levänen, *RSC Advances*, 2014, **4**, 61137-61152.
93 A. B. Hamidreza, B. S. Reza, C. S. Mahdi, D. Y. Mahdi, E. F. Fatemeh and F. H. Hassan, *Journal of Fundamental and Applied Sciences*, 2016, **8**, 839-859.
94 M. Wang, B. Zhao, S. Xu, L. Lin, S. Liu and D. He, *Chemical Communications*, 2014, **50**, 930-932.
95 M. Kinoshita and Y. Shimoyama, *The Journal of Supercritical Fluids*, 2016, **116**, 190-197.
96 J. F. Brennecke and C. A. Eckert, *AIChE Journal*, 1989, **35**, 1409-1427.
97 A. M. Scurto, K. Hutchenson and B. Subramaniam, in *Gas-Expanded Liquids and Near-Critical Media*, American Chemical Society, 2009, 1006, 1, 3-37.
98 M. J. Tenorio, S. Gines, C. Pando, J. A. R. Renuncio and A. Cabanas, *Journal of Chemical and Engineering Data*, 2018, **63**, 1065-1071.
99 A. Braeuer, S. Dowy, A. Leipertz, R. Schatz and E. Schluecker, *Optics Express*, 2007, **15**, 8377-8382.
100 D. L. Sparks, R. Hernandez and L. A. Estévez, *Chemical Engineering Science*, 2008, **63**, 4292-4301.
101 G. Sodeifian, N. Saadati Ardestani, S. A. Sajadian and H. S. Panah, *Fluid Phase Equilibria*, 2018, **458**, 102-114.
102 P. Caramazana-González, P. W. Dunne, M. Gimeno-Fabra, M. Zilka, M. Ticha, B. Stieberova, F. Freiberg, J. McKechnie and E. H. Lester, *Green Chemistry*, 2017, **19**, 1536-1547.
103 M. Tsang, G. Philippot, C. Aymonier and G. Sonnemann, *Green Chemistry*, 2016, **18**, 4924-4933.

